Nanoscale

PAPER

View Article Online
View Journal

Cite this: DOI: 10.1039/c5nr00045a

Thick solid electrolyte interphases grown on silicon nanocone anodes during slow cycling and their negative effects on the performance of Li-ion batteries

Fei Luo, Geng Chu, Xiaoxiang Xia, Bonan Liu, Jieyun Zheng, Junjie Li,* Hong Li,* Changzhi Gu and Liquan Chen

Thickness, homogeneity and coverage of the surface passivation layer on Si anodes for Li-ion batteries have decisive influences on their cyclic performance and coulombic efficiency, but related information is difficult to obtain, especially during cycling. In this work, a well-defined silicon nanocone (SNC) on silicon wafer sample has been fabricated as a model electrode in lithium ion batteries to investigate the growth of surface species on the SNC electrode during cycling using *ex situ* scanning electronic microscopy. It is observed that an extra 5 μm thick layer covers the top of the SNCs after 25 cycles at 0.1 C. This top layer has been proven to be a solid electrolyte interphase (SEI) layer by designing a solid lithium battery. It is noticed that the SEI layer is much thinner at a high rate of 1 C. The cyclic performance of the SNCs at 1 C looks much better than that of the same electrode at 0.1 C in the half cell. Our findings clearly demonstrate that the formation of the thick SEI on the naked nanostructured Si anode during low rate cycling is a serious problem for practical applications. An in depth understanding of this problem may provide valuable guidance in designing Si-based anode materials.

Received 5th January 2015,
Accepted 21st March 2015

DOI: 10.1039/c5nr00045a

www.rsc.org/nanoscale

Introduction

In order to satisfy the increasing demand for high energy density Li-ion batteries for various applications, high capacity alloy-type materials containing Sn,[1,2] Ge,[3–5] Ga[6,7] and Si[8–10] have been investigated widely to replace graphite anodes. Among all candidates,[11,12] silicon-based materials are the most promising due to their highest theoretical capacity of 3580 mA h g^{-1} for forming $Li_{15}Si_4$,[13,14] abundant sources, environmentally benign properties and low cost. Following comprehensive studies,[12,15–17] two problems become major challenges for practical applications. Firstly, the insertion of lithium will cause the expansion of the Si clusters/grains/particles unavoidably. The volume variation of the Si particles during lithiation and delithiation is linearly proportional to the Li-storage capacity and could reach 320% for full lithiation.[18] Such a conclusion is applicable to both crystalline and amorphous silicon. Drastic volume variations could lead to the cracking of large particles (>300 nm), the peeling off of active material layers from the current collector, the loss of electronic contact, the exposure of fresh surfaces in the electrolyte, and the destruction of the surface passivation films. In addition, most devices cannot allow significant expansion (<5–20%) of the battery inside. Consequently, the design of the Si-based electrode in Li-ion batteries has to consider this practical requirement and limit the total capacity or total volume variation of the electrode to an acceptable level.

Secondly, it has been found that the solid electrolyte interphase (SEI) layer on a silicon anode is very thick, inhomogeneous and unstable during electrochemical cycling.[19,20] The thickness of the SEI layer at the surface of silicon can be greater than 800 nm (based on the SEM image).[21,22] It is also noticed that the coverage of the SEI film could be as low as 60% after the first cycle.[20] Consequently, the initial coulombic efficiency is lower than 90%. The coulombic efficiency reaches over 99% after several cycles but cannot approach over 99.8% in successive cycles. This is more apparent for high surface area Si-based anodes. It has been found that Si-based anodes can show a much better cyclic performance in a half lithium cell than that in a full cell. In full Li-ion batteries, the cathode acts as the lithium source. Low coulombic efficiencies mean irreversible capacity loss. Therefore, lithium from the cathode will be consumed irreversibly which leads to fast capacity fading in the full battery. In addition, the formation of a thick SEI means the consumption of the electrolyte and the increase

Beijing National Laboratory for Condensed Matter Physics, Institute of Physics, Chinese Academy of Science, Beijing, 100190, China. E-mail: jjli@iphy.ac.cn, hli@iphy.ac.cn

of the internal resistance. Such a situation is not significant in the electrolyte-flooded half cell due to the excess lithium source and sufficient amount of electrolyte.

In view of fundamental research, it is necessary to understand the growth and coverage of the SEI on the Si anode during cycling. However, direct experimental investigations have rarely been reported due to the irregular and varied morphology of most Si-based anode materials.

Herein, an ICP cryogenic silicon etching method is developed to fabricate well-defined SNC arrays with a high aspect ratio on the full silicon wafer. This nanocone structure has several advantages for investigating the SEI film. Firstly, the SNCs are free of conductive additives and binders, thus eliminating the influence of conductive additives and binders on the growth of the SEI on the silicon anode. Secondly, the uniqueness of the high aspect ratio of the SNCs can offer free space to accommodate the volume change for maintaining a stable structure during electrochemical cycling. Thirdly, the SEM characterization for the silicon nano-particles (or amorphous Si thin films) is complicated by the fact that it is difficult to visually distinguish the SEI from the silicon region. The SNCs have the characteristic of regular appearance, which is favorable for the SEM observation.

Experimental

Materials

All reagents and solvents were used as received. Ethylene carbonate (EC, ≥99%), dimethyl carbonate (DMC, ≥99%), lithium hexafluorophosphate ($LiPF_6$, ≥99.99%) were purchased from Alfa Aesar. Silicon wafer (4 inches, p(100)) were purchased from Beijing Zhongjingkeyi Technology Co., Ltd.

SNC preparation

The SNCs were prepared through an etching process, carried out using cryogenic inductively coupled plasma (ICP) reaction ion etching, in which SF_6 and O_2 served as the etching gas at a low temperature (−120 °C). The formation of the silicon nanocone arrays firstly needs an anisotropic etching process, which is based on a competing etching and passivation process. Adequate balance between etching and passivation results in structures with perfectly vertical sidewalls, while excessive passivation results in the incomplete removal of the passivation layer from the etched field and inflicts micromasking, which plays a key role in further formation of the silicon nanocone structure.[23,24] As the etching proceeds, a random array of SNCs will form. In the etching process, the height, width, sloping angle and density of the SNCs could be tuned by selecting suitable plasma etching conditions, such as the process pressure, platen power, flow ratio (SF_6/O_2) and temperature. The SNCs before cycling were cut into electrodes with a size of 0.5 cm × 0.5 cm and vacuum dried for more than 5 h at 120 °C to remove moisture from the electrode.

Electrochemical testing

Swagelok-type two-electrode batteries were assembled in an Ar-filled glove box (MBraun, H_2O and O_2 <0.1 ppm). The SNCs were used as the working electrodes, and lithium foil was used as the counter electrode. The electrolyte was 1 mol L^{-1} $LiPF_6$ dissolved in ethylene carbonate (EC) : dimethyl carbonate (DMC) (1 : 1, v/v). Electrochemical cycling of the assembled half-batteries was performed by a Land BA2100A battery tester (Wuhan, China). All batteries were galvanostatically discharged (lithiated) to a limited capacity (100 μA h cm^{-2}) and charged (delithiated) to 2.0 V *vs.* Li^+/Li at room temperature. The current densities of 0.1 C, 0.5 C and 1 C are 10 μA cm^{-2}, 50 μA cm^{-2} and 100 μA cm^{-2}, respectively.

Assembly of the solid state battery (SSB)

The SSB was assembled in an Ar-filled glove box using the following steps: (1) the cell after the 25th cycle at 0.1 C was disassembled, and the separator between the SNC and the lithium foil was removed. (2) The SNC was washed by anhydrous DMC several times to make sure there was no residual $LiPF_6$. The SNC was vacuum dried for more than 5 h to make sure there was no residual solvent. (3) After the above treatment process, the SNC was used as a working electrode, and lithium foil was used as a counter electrode. In this battery, a 5 μm SEI layer on the SNC acted as the solid electrolyte.

Characterization

The batteries after the 1st, 2nd, 10th, 15th, 20th and 25th cycle at 0.1 C were disassembled in the Ar-filled glove box and the SNCs were washed by anhydrous DMC several times to make sure there was no residual $LiPF_6$, and then the samples were vacuum dried for more than 5 h to remove the solvent. The morphologies of the SEIs at the surfaces of the SNCs were observed by a Hitachi S-4800 scanning electron microscope (SEM) equipped with energy dispersive X-ray spectroscopy (EDS). The samples were sealed in a special vacuum transfer box during the sample transfer from the glove box to the SEM chamber.

Results and discussion

The aspect ratio of the as-fabricated SNCs is controlled by tuning the etching pressure as shown in Fig. 1a. The sample with the highest aspect ratio of 10 is chosen in this work due to its large space which can alleviate volume variation and avoid cracking[25,26] as well as possessing space for filling the SEI species. The half-width of each nanocone in the selected SNC sample is about 200 nm and the height of the Si nanocone layer is about 2.02 μm. The first charge (delithiation) capacity of the SNCs at 0.1 C can reach 83.5 μA h cm^{-2} (corresponding to a specific capacity of 1668 mA h g^{-1}, for $Li_{1.75}Si$, though this is a rough estimation). The coulombic efficiency in the initial cycle is 83.5% and increases to *ca.* 95% in the subsequent cycles. Fig. 1c exhibits the cycling performance of the SNCs at 0.1 C.

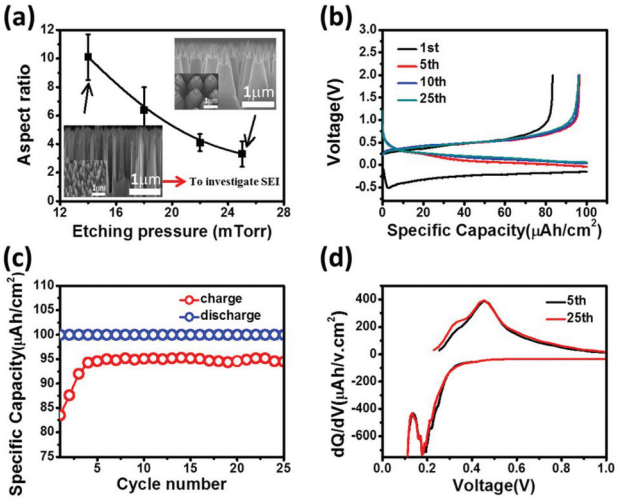

Fig. 1 (a) Aspect ratio of the as-fabricated SNCs *vs.* the process pressure; the inserted SEM images represent the highest (bottom left) and the lowest (top right) aspect ratio of the SNCs in this work. (b) Voltage *vs.* capacity profile of the SNCs at 0.1 C from the 1st to the 25th cycle. (c) The galvanostatic cycling performance of the SNCs (the current density is 10 μA cm^{-2}, discharge to the limited capacity at 100 μA h cm^{-2}). (d) Curves of d*Q*/d*V* for the SNC electrodes after the 5th and 25th cycles.

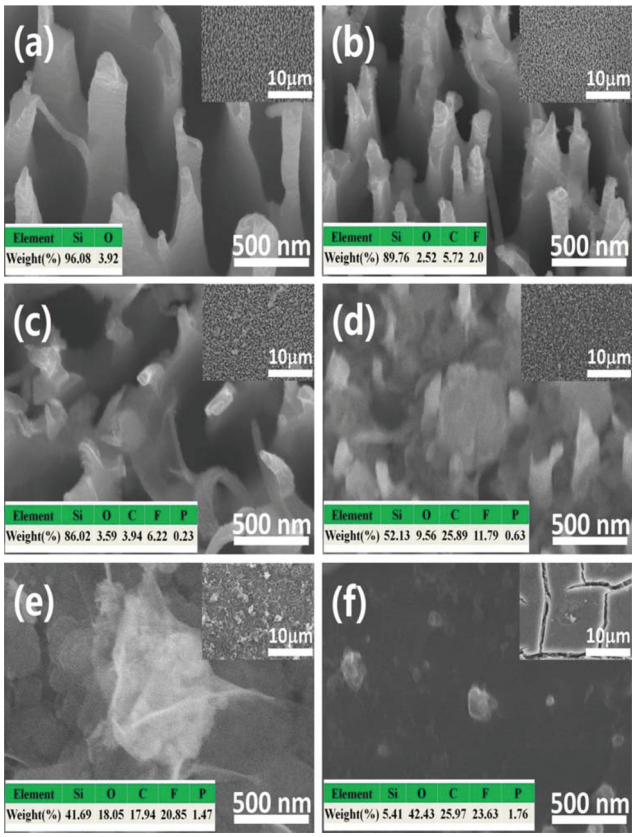

Fig. 2 SNC SEM images at (a) the 1st cycle, (b) the 2nd cycle, (c) the 10th cycle, (d) the 15th cycle, (e) the 20th cycle and (f) the 25th cycle. The bottom left inset of each SEM image shows the elemental concentrations of the SNCs, as determined by EDS. The top right inset of each SEM image is the surface morphology at low magnification.

During the first five cycles, the charge (delithiation) capacity increases gradually from 83.5 μA h cm^{-2} to 94.5 μA h cm^{-2}, indicating an activation process. In this work, the silicon nanocone electrode was prepared from a silicon wafer (4 inches, p(100)) through an etching process. The Si wafer (460 μm) acts as the substrate layer and the surface silicon nanocone layer has a thickness of 2 μm. Obviously, the Si wafer can also take part in the electrochemical reaction. The kinetics for the initial lithiation is difficult since both the Si wafer and the silicon nanocones have low electronic conductivities and a crystal-to-amorphous phase transition reaction occurs.[27,28] This is shown clearly in the differential capacity curves (Fig. 1d). One broad Li insertion (alloying) peak at 0.19 V, a peak below 0.19 V and two Li extraction (de-alloying) peaks at 0.32 V and 0.48 V can be seen. The appearance of two peaks in the d*Q*/d*V* curves is quite common in the Si-based anodes and can be explained by a two-step amorphous phase transition mechanism, as reported previously.[27,28] The similarity between the 5th and 25th differential capacity curves indicates that the electrochemical behavior of the SNCs is similar at the 5th and 25th cycles.

It can be seen from Fig. 1b that the activity of the Si wafer and the Si nanocones increases gradually upon cycling due to the increase of the electronic conductivity of lithiated Si and the structure variation.

The morphology of the SNC anodes at different cycles has been investigated by a SEM technique. A special sample transfer holder was used for the Hitachi 4800 microscope in order to transfer the lithiated samples from the glove box to the SEM vacuum chamber without exposure to air. After the first cycle, the morphology variation of the SNC electrode is not obvious (Fig. 2a) compared to the original sample (see Fig. 1a left inset). EDS analysis indicates that the atomic ratio of Si and O is 96.08% and 3.92%, respectively, without any presence of F and C. As we reported recently, the SEI may not cover the whole surface of the Si thin film electrode.[20] The absence of C and F means that the SEI content is very low and cannot be detected by EDS. This can be explained. Actually, the Si nanocone electrode has low electronic conductivity. As shown in the first discharge curve (Fig. 1b), the lithiation voltage is less than 0.0 V due to a very high initial polarization. In this experimental study, the discharge was performed by controlling the constant capacity. Therefore, lithiation is kinetically difficult, but still occurs after the voltage drops below 0.0 V. After the first discharge, the Si nanocone electrode is activated and the lithiated Si should have enhanced activity and electronic conductivity. Therefore, after the first cycle, the electrochemical behaviour of the Si nanocone electrode becomes normal. The first cycle can be understood as an activation process, although the detailed mechanism is still very clear.

After the second cycle, some granular particles are found on the SNCs (Fig. 2b). A top view shown in the inset of Fig. 2b

indicates that the electrode is well preserved. EDS analysis indicates the presence of Si, O, F, and C (89.76%, 2.52%, 2.0% and 5.72%, respectively), which is consistent with the deposition of the SEI. After the 10th cycle, the amount of granular SEI particles increases significantly and can be seen even on the top of the electrode (Fig. 2c, inset). EDS analysis of the electrode reveals that the concentrations of O, F, C, and P (3.59%, 6.22%, 3.94%, and 0.23%, respectively) increase significantly, indicating the increase of the SEI species. After the 15th cycle, the film-like species become more significant and the cavities between each individual Si nanocone evidently decrease compared to Fig. 2a. The atomic ratio of O, C, F and P increases to 9.56%, 25.89%, 11.79% and 0.63%, respectively.

After 20 cycles, no cavity can be seen from the top and the surface is covered completely. The atomic ratio of O, C, F and P increases to 18.05%, 17.94%, 20.85 and 1.47%, respectively. After the 25th cycle, some cracks can be seen from the top and the area without cracks seems quite flat. The atomic ratio of O, C, F and P increases to 42.43%, 25.97%, 23.63% and 1.76%, respectively.

The growth of the SEI species and the filling of the SEI species into the cavities between each Si nanocone can be clearly seen from the side views shown in Fig. 3. After 20 cycles, all cavities have been filled by the SEI species and the top layer becomes flat. Another extra layer covers the surface of the Si nanocone array electrode after the 25th cycle.

A magnified cross section image of the sample after the 25th cycle and the corresponding EDS mapping is shown in Fig. 4. Based on the cross section SEM images and EDS mapping of the SNCs after 25 cycles, the mean thickness from the bottom of the SNCs to the top of the SEI is 7.1 μm. The height of the SNC layer is about 2.02 μm. Thus, the distance between the top of the nanocones and the top of the SEI layer is 5.08 μm, very close to 5 μm. The top layer has a thickness of 5 μm and is composed of F, O, C, P and negligible amounts of Si. Therefore, it can be claimed undoubtedly that the top layer should be a SEI layer, which will be confirmed further in later sections by testing a solid battery.

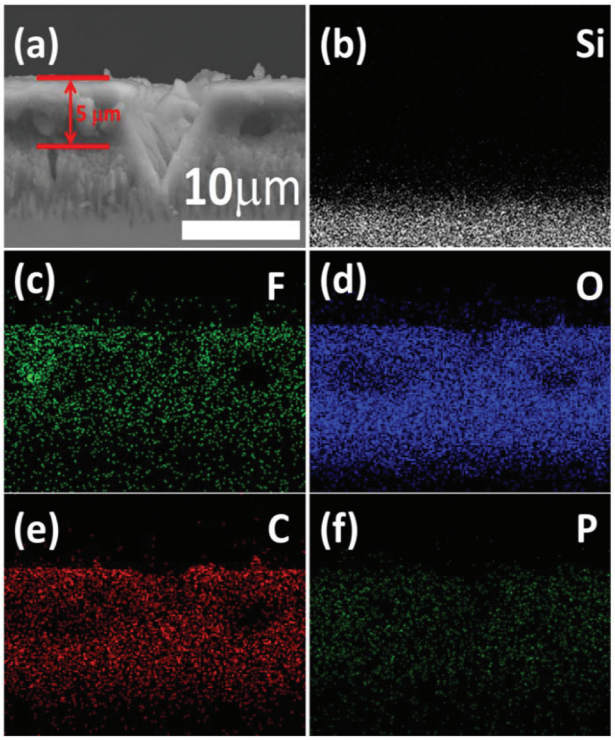

Fig. 4 Elemental mapping image of the cross section of the SNC after the 25th cycle.

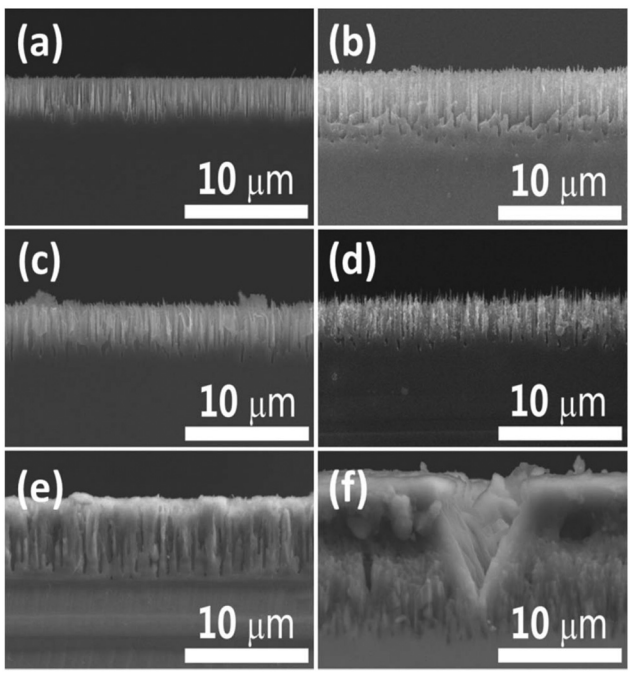

Fig. 3 Cross section SEM images of the SNCs at (a) the primary sample, (b) the 5th cycle, (c) the 10th cycle, (d) the 15th cycle, (e) the 20th cycle and (f) the 25th cycle.

According to Fig. 2–4, a scheme with insets of the SEI images at the side-view at different cycles is shown in Fig. 5. The SEI growth on the SNC electrodes includes five steps as follows:

(1) Nucleation of some granular SEI particles on the surface of the SNCs at the first two cycles (Fig. 5b).

(2) Aggregation of the granular SEI particles after the 10th cycle (Fig. 5c).

(3) Filling of the cavities between the SNCs after the 15th cycle (Fig. 5d).

(4) Further growth of the SEI and formation of an extra top layer after the 20th cycle (Fig. 5e).

(5) Growth to an extra 5 μm top layer.

(6) Cracking of the SEI layer after the 25th cycle (Fig. 5f).

The above results indicate two points:

(1) Complete coverage of the SEI layer on such nanostructured Si anodes needs many cycles.

(2) The thickness of the SEI layer can reach 5 μm.

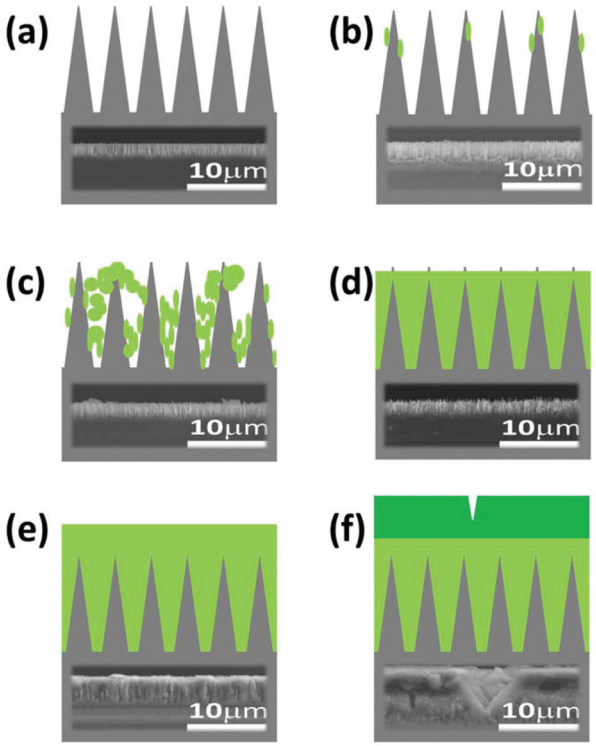

Fig. 5 The scheme of the procedure for forming the SEI on the SNC electrodes. The insets are the cross section SNC SEM images at (a) the primary sample, (b) the 2nd cycle, (c) the 10th cycle, (d) the 15th cycle, (e) the 20th cycle and (f) the 25th cycle.

Our recent force-curve investigation on the coverage of the SEI on Si thin film electrodes indicates that the SEI can only cover 60% of the surface area of a flat Si thin film electrode even after maintaining a constant potential at 5 mV *vs.* Li^+/Li in a half cell for 48 hours.[20] The incomplete coverage of the SEI layer could be due to several factors. One is inhomogeneous surface electronic conductivity. Once lithium is inserted into a certain area of the Si particles/electrodes, the local electronic conductivity increases sharply. This area could become more active for both lithium insertion and electrochemical reduction of the electrolyte compared to the unreacted Si areas. In addition, the growth of the SEI on the anode is a dynamic competition process between the nucleation of the SEI species, the dissolution of the SEI species and the deposition on the existing SEI layer or on a naked area. If the surface is inhomogeneous, then the nucleation and growth of the SEI is inhomogeneous.[20]

It is observed that the extra SEI top layer is as thick as 5 μm. It has been previously well accepted that the thickness of the SEI should be closed to the electron tunneling length. The effectiveness of this conclusion requires four presumptions:

(1) The SEI is dense;
(2) The growth of the SEI is homogeneous;
(3) The SEI is stable after growth;
(4) The SEI is electronically insulating.

Our recent investigations invalidate the first three presumptions.[20] The last one is still not clear since the direct measurement of the electronic conductivity of the SEI seems difficult (a conductive AFM or STM mapping may clarify this issue; we plan to do this in the near future). The thickness of the SEI above the electron tunneling path has also been observed in other anode materials.[21,22,29,30] In addition, the charge capacities still remain much lower than the discharge capacity even after 25 cycles, with the Coulombic efficiency around 95%. This means that the SEI layer could grow further even after 25 cycles unless the liquid electrolyte is exhausted or the SEI layer becomes compact enough when all the nanopores in the SEI are completely filled. In real Li-ion batteries, it is known that the SEI grows continuously even after 1000 cycles for a graphite anode. In many cases, the Li-ion batteries fail due to the exhaustion of the electrolyte in forming the SEI. A good material design should consider adding an effective SEI controlling additive or coating the anode to slow down this side reaction during cycling.

Many reports in the literature claim that nanosized or nanostructured Si anodes show excellent cyclic performance and rate performance, especially at high rates. It is interesting and valuable to investigate the growth of the SEI at high rates since it is convenient for our sample with a unique well-defined morphology.

Fig. 6a–d clearly show that the thick SEI film is not observed after 25 cycles both at 0.5 C and 1 C. The morphology of the SNC electrode at 0.5 C and 1 C after 25 cycles is close to that at 0.1 C after the 10th cycle and after the 2nd cycle, respectively. The EDS analysis of the SNCs at 0.5 C and 1 C described in Table 1 will give similar results. This suggests clearly that the higher the rate, the thinner the SEI after the same cycle.

The influence of the rate on the thickness of the SEI is not very clear. There could be three possible reasons:

(1) Reaction path: it has been reported that the reduction of the organic solvents could be either *via* a single-electron reaction at a low current density or a double-electron reaction at a high current density.[30,31] The former tends to form sparse alkyl carbonate, the latter tends to form dense Li_2CO_3. Such a mechanism has been well studied by Aurbach *et al.* previously.[31,32]

(2) Kinetics: the kinetics of the decomposition of the electrolyte is influenced by the current density. In this experimental study, the capacity is fixed. Lithiation and the formation of the SEI are two parallel reactions during discharging. At a high rate, the formation of the SEI may not follow.

(3) Chemical reaction: lithiated Si could react with solvents and salts chemically. This is known from the NMR results done by Grey *et al.*[33] At a high rate, the discharge period is much shorter than that at a low rate. Therefore, the period for a chemical side reaction is much more different. This will happen if the SEI is porous.

Up to now, there has been no direct quantitative experimental evidence to disclose the relationship between the SEI thickness and the rate. It is also not clear which factor plays the main role. This needs further clarification in the future.

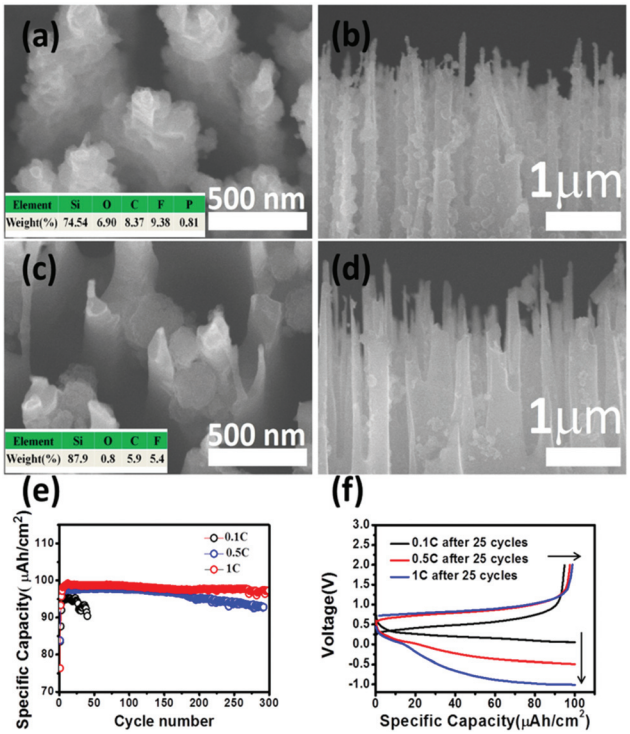

Fig. 6 (a) The SEM image of the SNC after the 25th cycle at 0.5 C (current density 50 μA cm^{-2}, discharge to the limited capacity at 100 μA h cm^{-2}). (b) The cross section SEM image of the SNC after the 25th cycle at 0.5 C. (c) The SEM image of the SNC after the 25th cycle at 1 C (current density 100 μA cm^{-2}). (d) The cross section SEM image of the SNC after the 25th cycle at 1 C. (e) The galvanostatic cycling performance of the SNC at 0.1 C, 0.5 C and 1 C. (f) The voltage *vs.* capacity profile of the SNC electrode after the 25th cycle at 0.1 C, 0.5 C and 1 C.

Table 1 EDS element mapping results of the SNC electrode at different states

State	Si	O	C	F	P
0.1 C, 1st	96.08%	3.92%	—	—	—
0.1 C, 2nd	89.76%	2.52%	5.76%	2.0%	—
0.1 C, 10th	86.02%	3.59%	6.22%	3.94%	0.23%
0.1 C, 15th	52.13%	9.56%	25.89%	11.79%	0.63%
0.1 C, 20th	41.69%	18.05%	17.94%	20.85%	1.47%
0.1 C, 25th	5.41%	42.43%	25.97%	23.63%	1.76%
0.5 C, 25th	74.54%	6.9%	8.37%	9.38%	0.81%
1 C, 25th	87.9%	0.8%	5.9%	5.4%	—

Fig. 6e shows that the SNC can achieve better cyclic performance at 1 C compared to 0.5 C and much better performance than that obtained at 0.1 C, under the same limited discharge capacity (100 μA h cm^{-2}). The reversible capacity after 300 cycles at 1 C remains at 97.3 μA h cm^{-2}, much higher than the value of 93 μA h cm^{-2} tested at 0.5 C, not mentioning the very poor cycling performance at 0.1 C. Remarkably, it should be mentioned that the average Coulombic efficiency during the first 25 cycles at 0.5 C and 1 C are 97.6% and 98.9%, respectively, both much higher than the value of 95% at 0.1 C. The above results confirm that the SNC can achieve superior cyclic performance and a high Coulombic efficiency at high rates. However, the same electrode shows poor performance at a low rate due to the continuous growth of the very thick SEI layer.

According to the above investigations, the growth of the thick SEI at a low rate is significant. It will consume the lithium from the cathode and the electrolyte in the full Li-ion battery irreversibly. Therefore, direct exposure of the Si surface to the electrolyte in non-aqueous Li-ion batteries should be avoided. Surface coating, forming a nanocomposite with a protective shell, and adding effective additives are recommended for the practical design.[34–36]

In the above discussion, we presume that the observed extra granular particles and the top coverage layer are the solid electrolyte interphase, however, except for EDS mapping, no direct evidence is provided to confirm that the top layer is the SEI. Actually, the SEI should play the role of a solid electrolyte. An experiment was designed to directly confirm that the top layer has the functionality of the SEI. After the 25th cycle, the half-cell was dissembled. A new solid cell was fabricated. The "SEI" covered SNC electrode was used as the cathode and the top "SEI" layer grown on the SNC electrode acted as the solid electrolyte. A fresh lithium foil was pasted on the top of the "SEI" covered SNC electrode. Then this Li/SEI/Si solid state battery (SSB) was cycled.

Fig. 7a shows the scheme of the cell and the electrochemical performances. The electrochemical test of this SSB was performed at a rate of 0.1 C (0.1 C = 10 μA cm^{-2}) at room temperature. As shown in Fig. 7b and c, the first reversible capacity is 31.6 μA h cm^{-2}. This value is 1/3 of the discharge

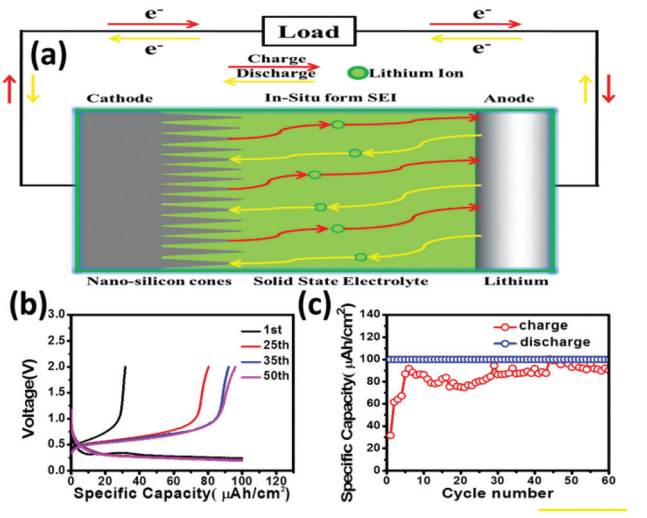

Fig. 7 (a) The schematic diagram of a solid state battery using the SEI formed *in situ* after 25 cycles in a Li/Si nanocone cell as the solid electrolyte; (b) the voltage *vs.* capacity profile of the SSB at 0.1 C from the 1st to the 50th cycle (current density 10 μA h cm^{-2}, discharge to the limited capacity at 100 μA h cm^{-2}); (c) the galvanostatic cycling performance of the SSB.

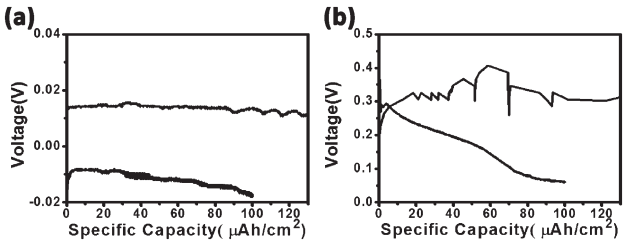

Fig. 8 (a) Charge and discharge curves of the SSB (solid state battery) using the primary SNC before cycling;, (b) charge and discharge curves of the SSB using the SNC after 10 cycles.

capacity (100 μA h cm^{-2}) using a liquid electrolyte. The reversible capacity increases to 86.2 μA h cm^{-2} in subsequent cycles. The increase of the capacity should be related to the improvement of the solid/solid interface. The main conclusion from this experiment is that the top "SEI" layer indeed has the functionality of a solid electrolyte layer: preventing electronic conduction but providing lithium ion conducting properties as an electrolyte.

It has to be mentioned that a similar cell could not operate if the top layer covered SNC electrode was replaced by the fresh SNC electrode (Fig. 8a), and could not operate properly when the SNC electrode was cycled only 10 times (Fig. 8b). The above results unambiguously confirm that the top 5 μm layer shown in Fig. 4a is the solid electrolyte interphase grown gradually on the SNC electrode during electrochemical cycling.

It is slightly surprising that this layer seems to have a high ionic conductivity since the prepared cell can operate at 0.1 C at room temperature and the polarization is not very high. The detailed chemical composition of this top SEI layer will be clarified in future by other techniques, such as SIMS, XPS and FTIR. This reminds us that this could be a new way to prepare a solid electrolyte or a way to introduce an artificial solid electrolyte in the composite solid lithium ion electrolyte.

Conclusions

SEM investigations of the morphology changes of the well-defined silicon nanocone array electrode in half cells at different cycles and rates indicate:

(1) The nucleation and growth of the SEI is inhomogeneous and full coverage of the SEI could be achieved after 10–20 cycles;

(2) The SEI could be as thick as 5 μm when the electrode is discharged at a low rate;

(3) The nanostructured Si nanocone electrode shows excellent cyclic performance and high Coulombic efficiency at a high rate in a half cell, but suffers at a low rate. This means that such a material cannot operate well in full batteries due to the irreversible and significant consumption of lithium from the cathode.

(4) The SEI layer grown during the electrochemical reactions really plays the role of the solid electrolyte. It can function well at room temperature. This may inspire us to design composite solid electrolytes.

Our findings indicate that direct contact of the Si-based anode material with the carbonate electrolyte should be avoided in Li-ion batteries, and the formation of a stable passivation layer on the Si-based anode before electrochemical discharging/charging is needed. Further investigations on the microstructure and chemical composition of such a thick SEI as well as the growth mechanism and kinetics are being carried out.

Acknowledgements

Financial support from NSFC project (51325206), "973" project of MOST (2012CB932900), "Strategic Priority Research Program" of the Chinese Academy of Sciences (XDA09010102) and Beijing S&T Project (Z131110000340000) is appreciated.

Notes and references

1 M. Noh, Y. Kwon, H. Lee, J. Cho, Y. Kim and M. G. Kim, *Chem. Mater.*, 2005, **17**, 1926–1929.
2 J. Hassoun, G. Derrien, S. Panero and B. Scrosati, *Adv. Mater.*, 2008, **20**, 3169–3175.
3 C. K. Chan, X. F. Zhang and Y. Cui, *Nano Lett.*, 2008, **8**, 307–309.
4 S. Yoon, C.-M. Park and H.-J. Sohn, *Electrochem. Solid-State Lett.*, 2008, **11**, A42–A45.
5 M. H. Park, Y. Cho, K. Kim, J. Kim, M. Liu and J. Cho, *Angew. Chem., Int. Ed.*, 2011, **123**, 9821–9824.
6 R. D. Deshpande, J. Li, Y.-T. Cheng and M. W. Verbrugge, *J. Electrochem. Soc.*, 2011, **158**, A845–A849.
7 W. Liang, L. Hong, H. Yang, F. Fan, Y. Liu, H. Li, J. Li, J. Y. Huang, L.-Q. Chen and T. Zhu, *Nano Lett.*, 2013, **13**, 5212–5217.
8 H. Li, X. Huang, L. Chen, Z. Wu and Y. Liang, *Electrochem. Solid-State Lett.*, 1999, **2**, 547–549.
9 N. Liu, H. Wu, M. T. McDowell, Y. Yao, C. Wang and Y. Cui, *Nano Lett.*, 2012, **12**, 3315–3321.
10 N. Liu, Z. Lu, J. Zhao, M. T. McDowell, H.-W. Lee, W. Zhao and Y. Cui, *Nat. Nanotechnol.*, 2014, **9**, 187–192.
11 U. Kasavajjula, C. Wang and A. J. Appleby, *J. Power Sources*, 2007, **163**, 1003–1039.
12 J. R. Szczech and S. Jin, *Energy Environ. Sci.*, 2011, **4**, 56–72.
13 X. H. Liu, H. Zheng, L. Zhong, S. Huang, K. Karki, L. Q. Zhang, Y. Liu, A. Kushima, W. T. Liang and J. W. Wang, *Nano Lett.*, 2011, **11**, 3312–3318.
14 J. Li and J. R. Dahn, *J. Electrochem. Soc.*, 2007, **154**, A156–A161.
15 Y. Yin, L. Wan and Y. Guo, *Chin. Sci. Bull.*, 2012, **57**, 4104–4110.

16 M. T. McDowell, S. W. Lee, W. D. Nix and Y. Cui, *Adv. Mater.*, 2013, **25**, 4966–4984.
17 X. Su, Q. Wu, J. Li, X. Xiao, A. Lott, W. Lu, B. W. Sheldon and J. Wu, *Adv. Energy Mater.*, 2014, **4**, 1–23.
18 Y. He, X. Yu, Y. Wang, H. Li and X. Huang, *Adv. Mater.*, 2011, **23**, 4938–4941.
19 C. K. Chan, R. Ruffo, S. S. Hong and Y. Cui, *J. Power Sources*, 2009, **189**, 1132–1140.
20 J. Y. Zheng, H. Zheng, R. Wang, L. Ben, W. Lu, L. Chen, L. Chen and H. Li, *Phys. Chem. Chem. Phys.*, 2014, **16**, 13229–13238.
21 P. H. L. Notten, F. Roozeboom, R. A. H. Niessen and L. Baggetto, *Adv. Mater.*, 2007, **19**, 4564–4567.
22 L. Baggetto, J. F. M. Oudenhoven, T. van Dongen, J. H. Klootwijk, M. Mulder, R. A. H. Niessen, M. H. J. M. de Croon and P. H. L. Notten, *J. Power Sources*, 2009, **189**, 402–410.
23 L. Sainiemi, H. Keskinen, M. Aromaa, L. Luosujärvi, K. Grigoras, T. Kotiaho, J. M. Mäkelä and S. Franssila, *Nanotechnology*, 2007, **18**, 505303.
24 H. Jansen, M. De Boer, S. Unnikrishnan, M. Louwerse and M. Elwenspoek, *J. Micromech. Microeng.*, 2009, **19**, 033001.
25 R. Ruffo, S. S. Hong, C. K. Chan, R. A. Huggins and Y. Cui, *J. Phys. Chem. C*, 2009, **113**, 11390–11398.
26 Y. He, X. Yu, Y. Wang, H. Li and X. Huang, *Adv. Mater.*, 2011, **23**, 4938–4941.
27 W. Yanhong, L. Yaoping, Z. Jieyun, Z. Hao, M. Zengxia, D. Xiaolong and L. Hong, *Nanotechnology*, 2013, **24**, 424011.
28 J. W. Wang, Y. He, F. Fan, X. H. Liu, S. Xia, Y. Liu, C. T. Harris, H. Li, J. Y. Huang, S. X. Mao and T. Zhu, *Nano Lett.*, 2013, **13**, 709–715.
29 K. F. Zhong, X. Xia, B. Zhang, H. Li, Z. X. Wang and L. Q. Chen, *J. Power Sources*, 2010, **195**, 3300–3308.
30 G. Gachot, S. Grugeon, M. Armand, S. Pilard, P. Guenot, J. M. Tarascon and S. Laruelle, *J. Power Sources*, 2008, **178**, 409–421.
31 D. Aurbach, B. Markovsky, M. D. Levi, E. Levi, A. Schechter, M. Moshkovich and Y. Cohen, *J. Power Sources*, 1999, **81–82**, 95–111.
32 K. Xu, *Chem. Rev.*, 2004, **104**, 4303–4418.
33 B. Key, R. Bhattacharyya, M. Morcrette, V. Seznec, J. M. Tarascon and C. P. Grey, *J. Am. Chem. Soc.*, 2011, **131**, 9239–9249.
34 H. Li, Z. Wang, L. Chen and X. Huang, *Adv. Mater.*, 2009, **21**, 4593–4607.
35 H. Li, J. Hu, X. J. Huang and L. Q. Chen, *Chinese patent*, ZL 1328805c, 2004.
36 H. Li and X. J. Huang, *Chinese patent*, ZL 100422112c, 2005.